EXPERIMENTAL STUDIES OF THE LEADING EDGE SUCTION FORCE, INCLUDING THE MAXIMUM ATTAINABLE SUCTION FORCE VERSUS REYNOLDS NUMBER AND THE INDUCED DISTRIBUTIONS ON VARIOUS WING PLANFORMS AND AIR INTAKES

Sven-Olof Ridder
Aeronautics Laboratory, Royal Institute of Technology
Stockholm, Sweden

Abstract

The effect of the Reynolds number on the maximum attainable leading edge suction force on a two-dimensional symmetrical wing was investigated at low speeds. The Reynolds number was varied by a factor 10 in the range where the laminar separation bubble strongly influences the flow.

In order to get a better understanding of the lift dependent drag problem the induced leading edge suction force distributions for various wing planforms, wing-fuselage configurations and air intakes were measured using a novel experimental technique.

Symbols and definitions

General

c	wing chord
L.E.	leading edge
R	leading edge radius
Re	Reynolds number
s	distance from the apex along the profile contour
$-X_i$	leading edge suction force
ν	kinematic viscosity
ϱ	density
σ	pressure rise coefficient

Pressure distribution symbols and definitions

K	factor for the leading edge singularity
p	static pressure
$q = \frac{1}{2}\varrho V^2$	dynamic pressure
t	maximum thickness of ellipse
V	stream velocity, positive direction away from the apex
x	distance from the apex in a chordwise direction
y	distance normal from the centerline of the profile
$C_p = 1-(V/V_\infty)^2$	incompressible pressure coefficient
$C_p = \frac{p-p_\infty}{q_\infty}$	experimental pressure coefficient
$[1-C_p]$	compressible near equivalence to the value $(V/V_\infty)^2$
C_L	lift coefficient
α	angle of attack

Indices

apex	value at the apex of the leading edge
i	induced by the flow around the leading edge
max	maximum value
st	stagnation point value
∞	free stream value
R	referred to the leading edge radius

Boundary layer symbols and definitions

h	maximum (displacement) height of the laminar bubble
$K_1 = \frac{t}{\theta}$	assumed to be constant throughout the bubble
K_2	factor for the velocity disturbance due to the displacement of the bubble
ℓ	length of the bubble
t	thickness of the separated shear layer of the bubble
u	stream velocity inside the boundary layer
U	stream velocity just outside the boundary layer
x	distance along the profile contour
y	distance normal to the profile contour
Δ	(small) increment
$\delta^* = \int_0^\infty (1-\frac{u}{U})\,dy$	displacement thickness of the boundary layer
$\theta = \int_0^\infty \frac{u}{U}(1-\frac{u}{U})dy$	momentum thickness of the boundary layer
τ_o	wall shearing stress

Indices

r	value at the point of reattachment
s	value at the point of separation

1. Introduction

It has long been recognized that for aerofoils of moderate thickness and camber the high lift characteristics at low speed may be strongly influenced by laminar separations of the boundary layer near the leading edge. The thickness of a laminar layer and the distance required for transition to turbulent flow is very much dependent on the Reynolds number and the same is accordingly true for the high lift characteristics when laminar separations are the critical factor.

The circulatory flow around a L.E. increases with increasing C_L, but the local flow condition i.e. pressure distribution is more directly related to the actual L.E. suction and the L.E. radius replaces the chord of the wing as the natural reference length.

The flow around a L.E. is associated with a suction peak immediately downstream the L.E. and in the subsequent region of pressure rise a laminar separation will usually occur. If the pressure gradient is strong and Re not too high a separated laminar shear layer is formed. After some distance downstream the initial point of separation a transition to turbulent flow takes place in the shear layer and provided the required pressure rise is not too high, reattachment as a turbulent boundary layer will follow.

This flow phenomenon is termed a laminar or short bubble and its effects on the pressure distribution is confined to the near vicinity of the bubble and the potential flow values of total forces and moments are only moderately affected.

If the separated shear layer fails to reattach immediately following transition, a long type of bubble may be formed if the pressure gradient is sufficiently reduced downstream on the wing chord, otherwise an open cavity flow will occur. The long bubble is turbulent in the greater part of its length and it has a major effect on the potential flow value of the net aerodynamic forces. Especially apparent is that the L.E. suction vanishes almost completely at the transition from short to long type of bubble or at the "bursting" of the laminar bubble.

The short bubble type of flow is found to exist at moderate angles of attack and Re. An increase of angle of attack or a decrease of Re may cause the bursting of the short bubble. This bursting happens quite abruptly and is also often associated with hysteresis effects.

From an aeronautical point of view the bursting of the laminar bubble invariably results in a sharp increase in drag, and in many cases also defines the maximum lift or sets the buffet boundaries. It should accordingly be helpful for performance predictions to investigate the factors that influence the maximum attainable L.E. suction force. Generally these factors should include L.E. geometry, Re and Mach number. The present study is only concerned with the effects of Re.

The flow around a L.E. on three-dimensional wings should basically be of a two-dimensional nature even for swept low aspect ratio wings when the short type of bubble flow is concerned. The characteristics corresponding to the long type of bubble flow, however, is very much dependent on the particular wing planform.

It should be justified to assume that the limiting conditions for the existence of the short type of bubble flow should in principle be applicable also on three-dimensional wings, especially at higher values of L.E. circulatory flow where the induced velocity components in a plane normal to the L.E. are of considerable magnitude compared with the free stream velocity.

In order to apply the two-dimensional data the detailed distribution of the L.E. suction forces on the actual three-dimensional wing has to be known. This distribution may be calculated with e.g. vortex lattice methods or be determined experimentally by measurements of the L.E. apex pressure. This latter method is briefly described and some typical results are presented at the end of this paper.

2. Inviscid flow around leading edges

2.1 Flat plate leading edge

The flat plate velocity distribution may be of the types represented by the full lines in the diagram below.

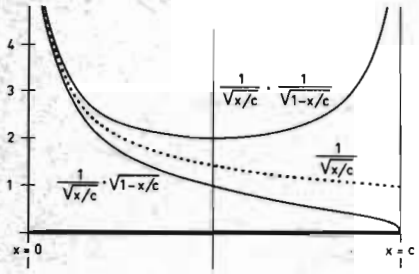

Taking the type that satisfies the Kutta condition at the trailing edge:

$$\frac{V}{V_\infty} = 1 \pm \frac{1}{\sqrt{x/c}} \cdot \alpha\sqrt{1-x/c}$$

or the symmetrical type approximating the effect of a narrow trailing edge flap:

$$\frac{V}{V_\infty} = 1 \pm \frac{1}{\sqrt{x/c}} \; K \; \frac{1}{\sqrt{1-x/c}}$$

and expanding in series gives

$$\frac{V}{V_\infty} = 1 \pm \frac{1}{\sqrt{x/c}} \; K \left[1 (\mp) \frac{1}{2} \, x/c + \ldots\ldots\ldots\ldots\right]$$

where the sign within brackets refers to the latter type of velocity distribution.

Close to the L.E. all types of velocity distributions can be approximated by:

$$\frac{V}{V_\infty} = 1 \pm \frac{K}{\sqrt{x/c}} = 1 \pm \frac{K}{\sqrt{x/x_{st}}}$$

using only the first term in the series expansion. The second term is the first order effect of the finite chord on the velocity distribution close to the L.E.

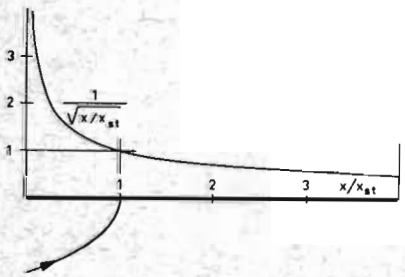

The L.E. suction force $-X_i$ is given by the zero drag condition of two-dimensional inviscid flow. For a flat plate:

$-X_i = 2 \pi q_\infty c \alpha^2$ assuming low angles of attack.

Also for a flat plate: $\alpha^2 = \dfrac{x_{st}/c}{1 - x_{st}/c}$

which can be simplified to:

$\alpha^2 = x_{st}/c$ when $x_{st}/c \ll 1$.

The L.E. suction force for a flat plate of infinite chord can thus be written:

$-X_i = 2 \pi q_\infty x_{st}$.

2.2 Parabolic leading edge

By application of Munk's rule [1] on the flow around a very slender ellipse at an angle of attack and with the rear stagnation point at the trailing edge, the approximate velocity distribution near the L.E. is found:

$$\frac{V}{V_\infty} = \frac{\sqrt{2\,x/R} \pm 2\,\alpha\,\sqrt{c/2R}}{\sqrt{1 + 2x/R}}$$

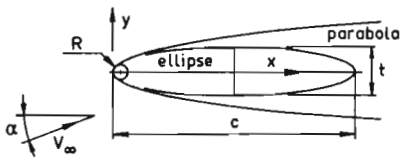

Defining the circulatory flow around the L.E. by the position of the forward stagnation point gives an expression that should be the exact solution for an infinite parabola:

$$\frac{V}{V_\infty} = \frac{\sqrt{2\,x/R} \pm \sqrt{2\,x_{st}/R}}{\sqrt{1 + 2\,x/R}}$$

The slender ellipse should have the same lift coefficient as the flat plate. The L.E. suction force is accordingly:

$-X_i = 2 \pi q_\infty c \alpha^2$

At the stagnation point:

$\sqrt{2\,x_{st}/R} = 2\alpha\sqrt{c/2\,R}$; $x_{st} = c\,\alpha^2$

The L.E. suction force becomes:

$-X_i = 2 \pi q_\infty x_{st}$ which is identical with the corresponding result for the flat plate.

The incompressible flow pressure coefficient is given by:

$$C_p = 1 - (V/V_\infty)^2$$

For the parabolic L.E.:

$$[1-C_p] = \frac{(\sqrt{2\ x/R} \pm \sqrt{2\ x_{st}/R})^2}{1 + 2\ x/R}$$

At the apex (x=0) $[1-C_p] = 2\ x_{st}/R$ and the L.E. suction force:

$$-X_i = \pi\ q_\infty\ R\ [1-C_p]_{apex}$$

For a parabolic L.E. it is sufficient to measure the pressure coefficient at one point (and most conveniently at the apex) in order to determine the L.E. suction force and the entire flow field in the L.E. region.

2.3 General symmetrical leading edges

The total velocity distribution in the L.E. region is principally made up by the following contributions:

1. Velocity due to thickness distribution

This part has zero velocity at the apex and for closed aerofoil shapes a maximum velocity is reached at some point along the contour. The maximum value increases with increasing bluntness of the L.E.

2. Velocity due to circulatory flow

This part is induced by the particular L.E. suction force that is required to satisfy the zero drag condition in combination with the actual normal force on the aerofoil.

It should be justified to assume that the circulatory flow component will be less dependent on the particular L.E. geometry. A fair approximation should be obtained from the velocity distribution of a parabola of equal L.E. radius and L.E. suction force.

The magnitude of the circulatory flow should best be described by the value of $(V/V_\infty)_{apex}$ or $[1-C_p]_{apex}$ rather than by the position of the stagnation point.

3. Velocity due to finite chord

This part is the linear term in the series expansion as derived for the flat plate.

Taking this trailing edge effect into account should improve the accuracy somewhat further downstream of the L.E. approximation of the velocity distribution.

The relative importance of the listed types of velocity contributions is shown in the diagram below at various values of $(V/V_\infty)_{apex}$

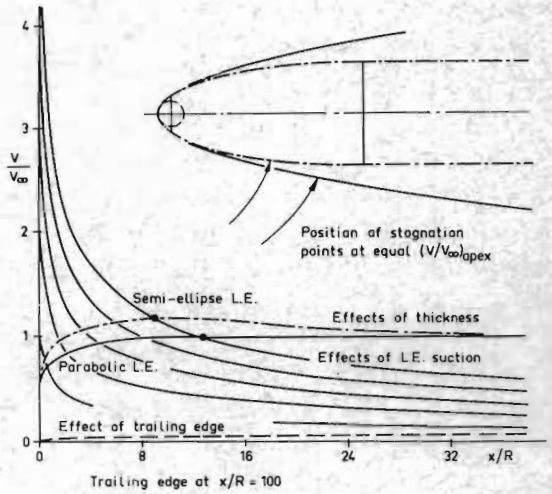

3. Boundary layer calculations

The boundary layers have been calculated for an infinite parabolic L.E. using the inviscid velocity distributions at various values of $[1-C_p]_{apex}$ and various values of Re.

For the calculations was used a numerical computer program developed by William D. McNally [4]. This program calculates the laminar boundary layer from the stagnation point to the separation point and in order to proceed, instantaneous transition to turbulent boundary layer has to be assumed.

For the present calculations continuity in the boundary layer momentum thickness was prescribed.

The primary calculated values have been used to interpolate the values of θ for those combinations

of $[1-C_p]_{apex}$ and Re which were experimentally found to be critical or near critical with respect to the maximum attainable L.E. suction force. These results are shown (dashed) in figure 12.

4. Description of the wind tunnel model, test equipment and procedures.

For the experimental studies a semi-ellipse L.E. was chosen as a practical shape and the central part of the wing was of constant thickness. The wing was provided with a single slotted trailing edge flap. The L.E. radius was 1 cm and the eccentricity of the full ellipse was 4:1. The chord of the wing was 161 cm including the 25 % trailing edge flap.

The model was installed in a two-dimensional insert in the low speed tunnel L2 of The Division of Aeronautics of The Royal Institute of Technology, Stockholm, as shown in figure 1. This tunnel has a closed, octagonal test section of 2 x 2 m^2.

In order to cancel the effect of the finite chord on the L.E. pressure distribution the deflection of the trailing edge was linked to the angle of attack rotation of the model in such a way that both the angle of attack and the deflection of the trailing edge flap contributed equally to the induced L.E. suction force. (See shapter 2.1.)

The tests were started with recordings of the L.E. apex pressure during continuous increase of the angle of attack up to the stall followed by a decrease of α until reattachment of the L.E. flow seemed to occur. This procedure was performed for a range of Re that was varied by a factor 10. For a set of Re the surface pressure distributions were measured at fixed values of $[1-C_p]_{apex}$ up to the critical (stalling) L.E. loading.

Boundary layer profiles were recorded downstream the laminar bubble and in some cases also within the bubble.

5. Experimental results

5.1 Surface pressure measurements

Fig 2. Effects of free stream dynamic pressure $[kp/m^2]$ on the L.E. apex pressure coefficient vs angle of attack

For reasons of clarity only the results for a few of the dynamic pressures tested are presented. At low angles of attack all the curves adhere well to the theoretical parabola, but at higher α the curves for lower dynamic pressures fall considerably below, as is probably caused by the comparatively thicker boundary layer on the rear part of the wing.

At a certain critical angle of attack the value of $[1-C_p]_{apex}$ drops abruptly to a much lower level indicating a complete flow breakdown in the L.E. region.

The maximum attainable value of $[1-C_p]_{apex}$ prior to flow breakdown grows very rapidly with increasing dynamic pressure.

Fig 3. Effect of Reynolds number on the maximum attainable L.E. suction

Re is in this context based on the L.E. radius and the free stream velocity. For increasing α there is at low to moderate Re an ever increasing slope of the curve up to $Re_R = 8.5 \cdot 10^3$. At higher Re the slope of the curve is decreased and the relationship appears almost linear.

For decreasing α the effect of Re is less pronounced and the distance between the two branches of the curve increases very rapidly with Re. The two types of L.E. flow represented by the two curves appeared to be very stable within their regimes, and the reproduction of flow separation and reattachment was very consistent.

Figs 4, 5 and 6. Effects of the magnitude of the circulatory flow around a L.E. on the pressure distribution

The surface pressure distribution for the lowest and the highest Re tested are presented at fixed values of $[1-C_p]_{apex}$ up to near the maximum attainable value of $[1-C_p]_{apex}$. The distributions exhibit the

characteristical suction peak downstream the L.E. according to inviscid theory.

A strictly experimental feature is noted in the region immediately downstream the suction peak with a zone of more or less constant pressure terminated by a rather steep pressure rise. This "bump" in the otherwise regular pressure distribution is the manifestation of the laminar separation bubble. At high Re the bubble is quite short, but at low Re the term short bubble would appear somewhat misleading.

Shown dotted in the region of the bubble is the attached flow pressure distribution that was calculated with an approximate method using the experimental velocity distribution of the semi-ellipse L.E. at zero angle of attack and the theoretical circulatory velocity distribution for a parabola.

Fig 7._ Relative pressure distributions of the laminar separation bubbles at near maximum L.E. suction vs surface contour

From the set of pressure distributions recorded for each particular Re are selected the ones representing near maximum L.E. suction force. The relative pressure distribution of the laminar separation bubbles are derived by dividing the value of $[1-C_p]$ (coefficient referred to the free stream dynamic pressure) by $[1-C_p]_s$ in order to relate all the pressure distributions to the local external stream pressure at separation.

It is evident that the three distributions for the lower Re are more affined than for higher Re.

Fig 8._ Relative pressure distributions of the laminar separation bubbles at near maximum L.E. suction vs local Re

The same set of pressure distributions as presented in figure 7 is further evaluated in the way that the coordinates of the surface contour are multiplied by the local velocity in the external flow at the laminar separation and divided by the kinematic viscosity so as to form a local Re.

This way of presentation makes the length of the separation bubbles about the same supporting the concept of Doenhoff [2], of a certain critical Re for transition of the separated laminar boundary layers based on local velocity and length along the flow.

It should be recognized that the set of laminar bubbles studied are not of identical proportions. The thickness of the separating boundary layer for instance is relatively smaller compared with the length of the bubble for low Re than for high Re. This initial thickness of the separating shear layer seems to be a factor of secondary importance regarding the effect on the length of the bubble.

The length of the near constant pressure region seems to be approximatley two thirds of the total length of the bubble. In the region of reattachment the shape of pressure distribution curves are fairly rounded which makes it somewhat difficult to define the length of the bubble accurately. The typical Re of the total length of the bubble is about $3.5 \cdot 10^4$ according to the present measurements. This value is obtained for a model with polished surface and with a free stream turbulence of 0.7 ‰ RMS in the test section.

Fig 9._ Pressure rise coefficients for laminar separation bubbles vs $[1-C_p]_{apex}$ at different Re

From all the recorded pressure distributions of the present investigation are compiled the pressure rise coefficients $\sigma = 1 - \frac{[1-C_p]}{[1-C_p]_s}$

For low values of circulatory L.E. flow it is evident that the value of σ increases rapidly with decreasing Re and increasing circulatory L.E. flow. At higher values of $[1-C_p]_{apex}$ this trend is changed in the way that the effect of circulatory flow is diminished and almost absent, but that the effect of Re remains about the same.

For low Re the σ-curves seem to be cut off by a maximum limit near the value of $\sigma_{max} = 0.35$ as found by Crabtree [3].

At higher values of $[1-C_p]_{apex}$ the flow conditions for the laminar bubble is discussed in the following way.

The equation for the pressure distribution of a parabolic L.E. is written: (see chapter 2.2)

$$[1-C_p] = \frac{(\sqrt{2x/R} \pm \sqrt{2x_{st}/R})^2}{1 + 2x/R} = \frac{(\pm y/R \mp y_{st}/R)^2}{1 + (y/R)^2}$$

At very high values of L.E. circulatory flow the suction peak will occur close to the apex of the L.E., Near the apex y/R may be neglected compared with y_{st}/R in the above expression.

A new pressure coefficient is related to the local dynamic pressure at the apex instead of to the free stream value:

$$\frac{[1-C_p]}{[1-C_p]_{apex}} \approx \frac{1}{1 + (y/R)^2}$$

For small values of y/R:

$$\frac{[1-C_p]}{[1-C_p]_{apex}} \approx 1 - (y/R)^2$$

A pressure rise coefficient σ' similar to σ as used for the study of laminar separations is introduced:

$$\sigma' = 1 - \frac{[1-C_p]}{[1-C_p]_{apex}} \approx (y/R)^2$$

Near the apex $y/R \approx s/R$ and accordingly $\sigma' \approx (s/R)^2$.

This way of reasoning proves that at high values of circulatory flow the pressure distributions near the L.E. apex tend to approach one universal type. If the circulatory flow is increased at constant Re (related to the free stream velocity) the local velocity at the laminar separation will increase and the length of the laminar bubble will be reduced. The pressure rise coefficient required to attain reattachment of the laminar separation is correspondingly reduced.

The conclusion is that above a certain $[1-C_p]_{apex}$ the laminar bubble will be progressively more lightly loaded by increasing L.E. suction, contrary to what is experienced at low values of circulatory L.E. flow and to what more directly appeals to the intuition.

5.2 Boundary layer measurements

For the combination of Re and $[1-C_p]_{apex}$ that were found to represent near maximum L.E. suction according to the present investigation, the boundary layer profiles were recorded by means of a total head probe mounted on a continuously movable traversing mechanism.

Fig 10. Displacement thickness of the boundary layers at near maximum L.E. suction for different Re

The diagram shows that the boundary layer is considerably thicker near the L.E. for low Re than for high Re. Further downstream on the aerofoil contour the situation is reversed i.e. with a thicker boundary layer at high Re and vice versa.

For the case of $Re_R = 6.1 \cdot 10^3$ (with a fairly long laminar bubble) four boundary layer stations within the bubble were recorded. The bubble itself is clearly indicated by the measurements but also immediately downstream there is evident a permanent increase in thickness of the reattaching turbulent boundary layer.

The difference in boundary layer thickness far downstream should be explained by the much higher degree of pressure recovery at the higher Re that offsets the natural trend to thinner boundary layer at high Re. (See figure 7.)

Fig 11. Momentum thickness of the boundary layers at near maximum L.E. suction for different Re

The momentum thickness of a separating shear layer should be constant in the constant pressure region immediately downstream the separation point if no frictional forces were acting. The experimental results for the case of $Re = 6.1 \cdot 10^3$ show a moderate increase of the momentum thickness in the forward part of the laminar bubble indicating the presence of a small amount of friction.

At the rear end of the bubble the experimental data is unfortunately a bit scarce but there is evidence of a rather abrupt increase in the momentum thickness of the reattaching shear layers. The magnitude of this increase seems to be roughly proportional to the length of the bubble. The existence of a very long laminar bubble at low Re is evidently associated with a very large initial thickness of the turbulent boundary layer.

Fig 12. Calculated momentum thickness of the boundary layers for reattaching bubbles

The data from figure 11 is reproduced at a magnified scale to more accurately show the details in the immediate vicinity of the laminar bubbles. The calculated momentum thickness data in the region of the apex for a parabolic L.E. is also shown (dashed).

These boundary layer calculations are based on the assumption of instantaneous transition to turbulent flow at the laminar separation point at constant momentum thickness. This assumption leads evidently to a serious misrepresentation of the real boundary layer development. The momentum thickness at the reattachment point is underestimated to approximately 50-60% of the real value.

At the forward end of the bubble the agreement between calculated and experimental data is fairly satisfactory but the calculated laminar separation points are closer to the L.E. than the experimental positions as can be interpreted from pressure distribution data (figure 7).

Separation bubbles having the same value of the pressure rise coefficient σ should in principle be geometrically congruent with respect to the displacement thickness in order to produce the same relative pressure rise. If the similarity also includes the velocity profiles at corresponding stations of the bubbles, the momentum thickness too will be proportional to the length of the bubble for bubbles having the same value of σ. This way of reasoning is expanded in chapter 6. The results from calculations of the increase in momentum thickness of reattaching separation bubbles are also presented in the diagram. The method would seem to predict the initial thickness of the turbulent boundary layer fairly well for the range of Re investigated.

In the diagram are also shown the measured velocity profiles of the separation bubble at $Re = 6.1 \cdot 10^3$ with the same scale for horizontal and vertical dimensions.

6. Schematic analysis of the increase in boundary layer thickness associated with the reattachment of bubble flow

Assumptions: Laminar separation occurs in a decelerating flow. The quantities δ_s and θ_s of the separating boundary layer are known. The velocity distribution for attached flow is also known. The length of the separation bubble is defined by a certain Re based on the local velocity outside the boundary layer at separation and a streamwise distance.

The bubble has a forward part with constant pressure followed by a rear part with a linear drop of velocity outside the bubble. The skin friction is zero within the bubble.

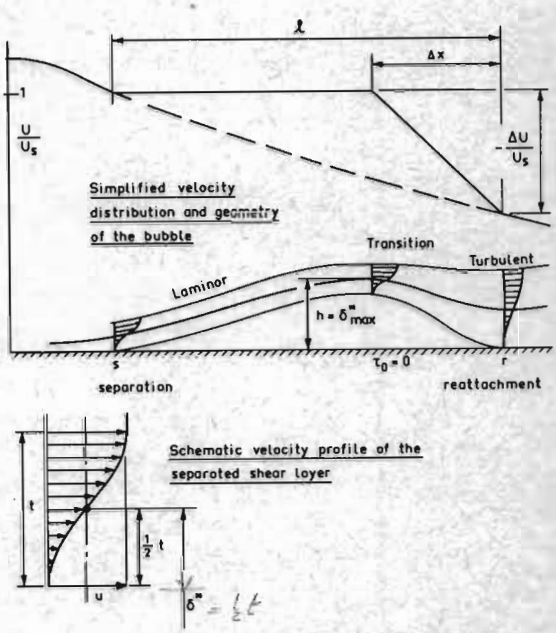

The type of velocity distribution of the free shear layer is assumed to be constant from separation to reattachment and of an antisymmetric form. $\Rightarrow \delta^* = \frac{1}{8}t$

Then: $\theta = \frac{t}{K_1}$ where K_1 is constant throughout the bubble.

The momentum thickness θ_s of the separated shear layer should be constant along the forward part of the bubble with constant pressure and also the thickness t of the shear layer should be constant with the assumed type of constant velocity profile.

The change in velocity $-\frac{\Delta U}{U_s}$ at the rear end of the bubble is prescribed in order to conform to the attached flow velocity distribution behind the bubble.

The shape of the bubble is determined by the requirement to keep the velocity constant outside the forward part of the bubble in the otherwise decelerating velocity field. Thus the relative thickness, taken as the maximum change in boundary layer displacement thickness along the bubble divided by the length of the bubble, should be proportional to the relative change in velocity $-\frac{\Delta U}{U_s}$

$$-\frac{\Delta U}{U_s} = \frac{K_2}{\ell}\left[h - \frac{1}{2}(\delta_s^* + \delta_r^*)\right] \qquad (1)$$

The von Kármán integral relation for a boundary layer is written in the form:

$$\frac{d\theta}{dx} + \frac{2\theta + \delta^*}{U}\frac{dU}{dx} = \frac{\tau_0}{\varrho U^2} \qquad (2)$$

This relation is applied to the reattachment of the flow at the rear end of the bubble. Equation (2) is multiplied by Δx and the mean values are formed:

$$\bar{\theta} = \theta_s + \frac{1}{2}\Delta\theta \qquad \bar{\delta}^* = \frac{1}{2}(h + \delta_r^*)$$

$$\bar{U} = U_s + \frac{1}{2}\Delta U \qquad \text{and} \qquad \tau_0 = 0$$

$$\Delta\theta = -\frac{\Delta U}{\bar{U}}(2\bar{\theta} + \bar{\delta}^*) =$$

$$= \frac{-\frac{\Delta U}{U_s}}{1 + \frac{1}{2}\frac{\Delta U}{U_s}}\left(2\theta_s + \Delta\theta + \frac{1}{2}h + \frac{1}{2}\delta_r^*\right) \qquad (3)$$

At reattachment:

$$\delta_r^* = \frac{1}{2}t_r = \frac{K_1}{2}(\theta_s + \Delta\theta) \qquad (4)$$

Equations (1) and (4) give:

$$h = -\frac{\Delta U}{U_s}\frac{\ell}{K_2} + \frac{1}{2}\delta_s^* + \frac{K_1}{4}(\theta_s + \Delta\theta) \qquad (5)$$

Using equations (4) and (5) in equation (3) gives:

$$\Delta\theta = \frac{-\frac{\Delta U}{U_s}}{1 + \frac{1}{2}\frac{\Delta U}{U_s}}\left[2\theta_s + \Delta\theta + \frac{K_1}{4}(\theta_s + \Delta\theta) + \right.$$

$$\left. + \frac{K_1}{8}(\theta_s + \Delta\theta) + \frac{1}{4}\delta_s^* - \frac{\Delta U}{U_s}\frac{\ell}{2K_2}\right] \qquad (6)$$

Putting $\delta_s^* = 2.31\,\theta_s$ (laminar separation) gives:

$$\Delta\theta = \frac{-\frac{\Delta U}{U_s}\left(2.578 + \frac{3K_1}{8}\right)}{1 + \frac{\Delta U}{U_s}\left(\frac{3}{2} + \frac{3K_1}{8}\right)}\theta_s + \frac{\left(\frac{\Delta U}{U_s}\right)^2\frac{1}{2K_2}}{1 + \frac{\Delta U}{U_s}\left(\frac{3}{2} + \frac{3K_1}{8}\right)}\ell \qquad (7)$$

The constant K_2 should be of the order of 4 as could e.g. be deduced from comparisons with velocity distribution data for symmetrical aerofoils.

The constant $K_1 = 2\frac{\delta_r^*}{\theta_r}$ should be of the order of 4 to 5.

With the assumption $K_2 = 4$, the value of K_1 is calculated to conform to experimental data at $Re_R = 6.1 \cdot 10^3$

From equation (7):

$$K_1 = \frac{\Delta\theta\left(-\frac{U_s}{\Delta U} - \frac{3}{2}\right) - 2.578\,\theta_s + \frac{\Delta U}{U_s}\frac{\ell}{2K_2}}{\frac{3}{8}(\theta_s + \Delta\theta)} \qquad (8)$$

With the experimental values:

$\theta_r = 0.47$ mm, $-\frac{\Delta U}{U_s} = 0.1876$ ($\sigma = 0.34$),

$\ell = 24$ mm and the calculated value $\theta_s = 0.06$ mm

and accordingly $\Delta\theta = 0.41$ mm

From the above data $K_1 = 4.840$

Assuming that the value of K_1 is representative for any reattaching laminar bubble, equation (7) can be expressed as:

$$\Delta\theta = \frac{1}{1 + 3.315\frac{\Delta U}{U_s}}\left[-4.393\frac{\Delta U}{U_s}\theta_s + \frac{1}{8}\left(\frac{\Delta U}{U_s}\right)^2\ell\right] \qquad (9)$$

Equation (9) has been used to calculate the increase in boundary layer momentum thickness based on the calculated thickness at the laminar separation and the length and pressure rise of the bubble according to measurements as presented in figure 7.

The calculated values of θ_r are presented in figure 12 where also the measured boundary layer momentum thickness data is plotted.

7. Leading edge suction on three-dimensional wings

The simple and linear relationship between the L.E. apex pressure and the local L.E. suction force for attached (short bubble) flow is used for a simple experimental technique [5] to measure the distribution of the tangential L.E. suction forces on thin plane wings and "thin walled" air intakes. For the practical application is employed a small, calibrated L.E. element with a very small pressure hole in the form of a narrow slit ($\approx$0.01 mm wide) at the apex of the symmetrical L.E.. The basic wing has a segmented L.E. of constant absolute section and any of these segments can be substituted by the special calibrated L.E. element.

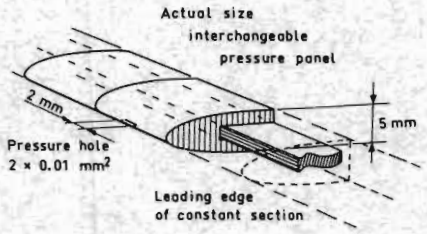

The apex pressure hole is connected to a pressure transducer (of small volume) and the test procedure consists in recording the variation of apex pressure during slow and continuous change of angle of attack within the range available for short bubble type of L.E. flow. The result is a fairly regular parabola for the pressure signal versus angle of attack.

The steepness of the parabola or the value of $[1-c_p]_{apex}/\alpha^2$ is a measure of the relative L.E. suction loading at the particular station along the L.E.

Based on the information regarding the distribution of the L.E. suction forces on the various aircraft components it should be possible to design the complete aircraft with the optimum use of arrangements intended for the conservation of attached L.E. flow i.e. L.E. radius-, L.E. camber- and L.E. flap-chord distributions.

Figure 13 shows the measured distributions of the L.E. suction forces on a 60° delta wing, alone and in combination with circular section fuselages of different sizes.

Figure 14 presents the effect of varying wing sweep angle on the L.E. suction forces distributions for a swept wing panel mounted as a high wing on a fuselage.

Figure 15 shows the L.E. suction forces distributions on a Viggen-type of configuration including the effect of the canard surface.

Figures 16 and 17 offer comparisons of the effects of angle of attack on the lip suction load of semi-circular air intakes at various positions in relation to the aircraft configuration.
(Inflow number = 1)

Conclusions

The effect of Re on the maximum attainable L.E. suction force is evident by a review of the diagram in figure 3.

At low Re the flow mechanism of reattachment of the laminar bubble is primarily critical ($\sigma < 0.35$)

At high Re the maximum attainable L.E. suction force is limited by separations further downstream of the reattached turbulent boundary layer. The main influence of the laminar bubble for this condition should be on the initial thickness of the turbulent boundary layer behind the bubble.

Regardless of which type of flow mechanism that causes the stall, exceeding the critical L.E. suction force results in a sudden flow breakdown with a long separation bubble starting near the L.E. apex. The propagation of the flow separations can not be observed using conventional flow visualization technique.

From other wind tunnels tests on high lift aerofoils it is experienced that sometimes improvements in $C_{L_{max}}$ can be obtained by the use of roughness elements near the L.E.. It seems likely that this method should be most successful in the lower Re-range where the length of the separation bubble is critical for the reattachment process. These roughness elements are to be placed upstream the laminar separation, probably somewhere between the L.E. apex and the suction peak. The effect of these transition devices can be either to suppress laminar separations entirely or to reduce the length of the bubble depending on Re and the size and distribution of the roughness elements.

At higher Re, when the thickness of the turbulent boundary layer is critical, the effect of the roughness elements to reduce the length of the bubble may be offset by the increase in momentum thickness caused by the drag of the projecting obstacles.

References

[1] Munk. Max. M.

Fluid Mechanics, Part II. Vol. I of Aerodynamic Theory. div. C, ch. VIII, sec.4

W.F. Durand. ed., Julius Springer (Berlin), 1935.

[2] Doenhoff. A.E.

A preliminary investigation of boundary layer transition along a flat plate with adverse pressure gradient.

NACA TN 639, March 1938.

[3] Crabtree. L.F.

Effects of leading-edge separation on thin wings in two-dimensional incompressible flow.

Journal of the Aeronautical Sciences, Aug. -57

[4] Mc Nally. William D.

FORTRAN program for calculating compressible laminar and turbulent boundary layers in arbitrary pressure gradients.

NASA TN D 5681, May 1970.

[5] Ridder, S-O

Experimental study of induced drag and leading edge tangential suction force spanwise distribution of thin plane delta wings at low speeds including the effects of fuselage diameter.

KTH AERO TN 58, Stockholm, May 197?.

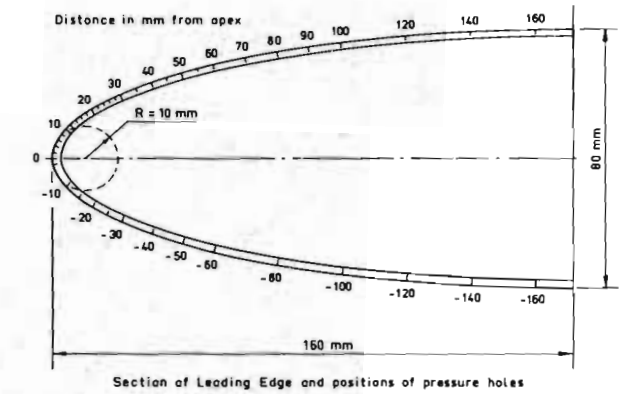

Section of Leading Edge and positions of pressure holes

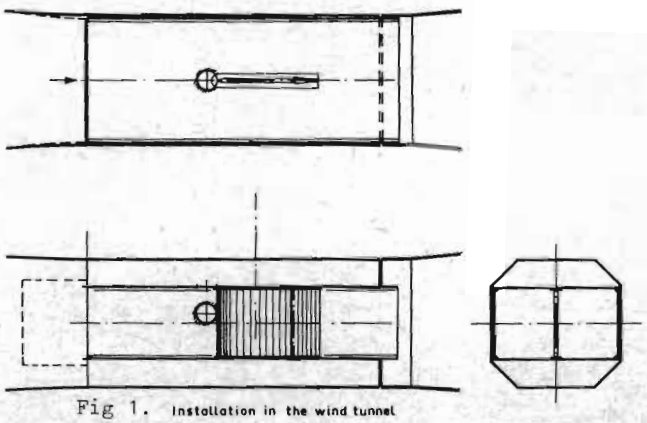

Fig 1. Installation in the wind tunnel

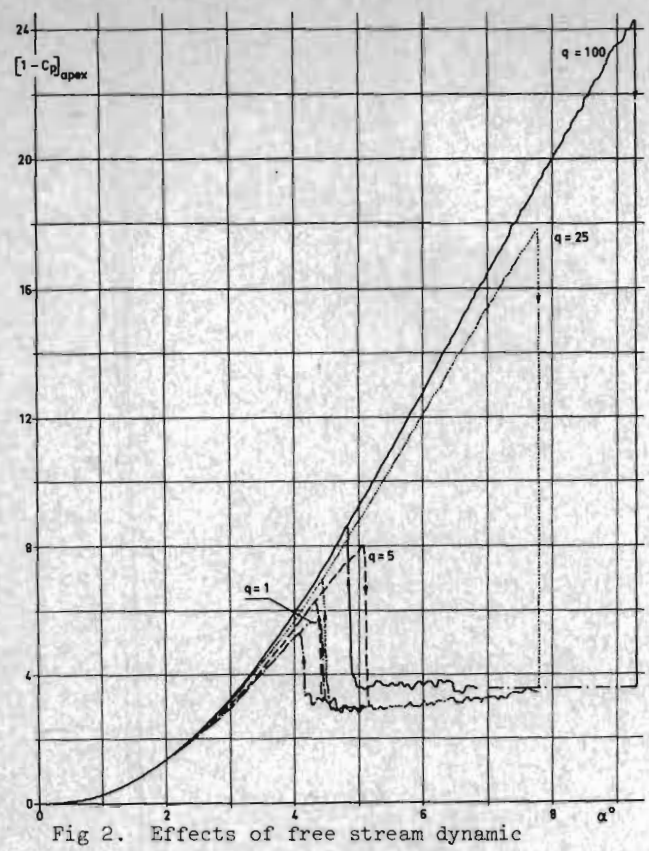

Fig 2. Effects of free stream dynamic pressure kp/m² on the L.E. apex pressure coefficient vs angle of attack.

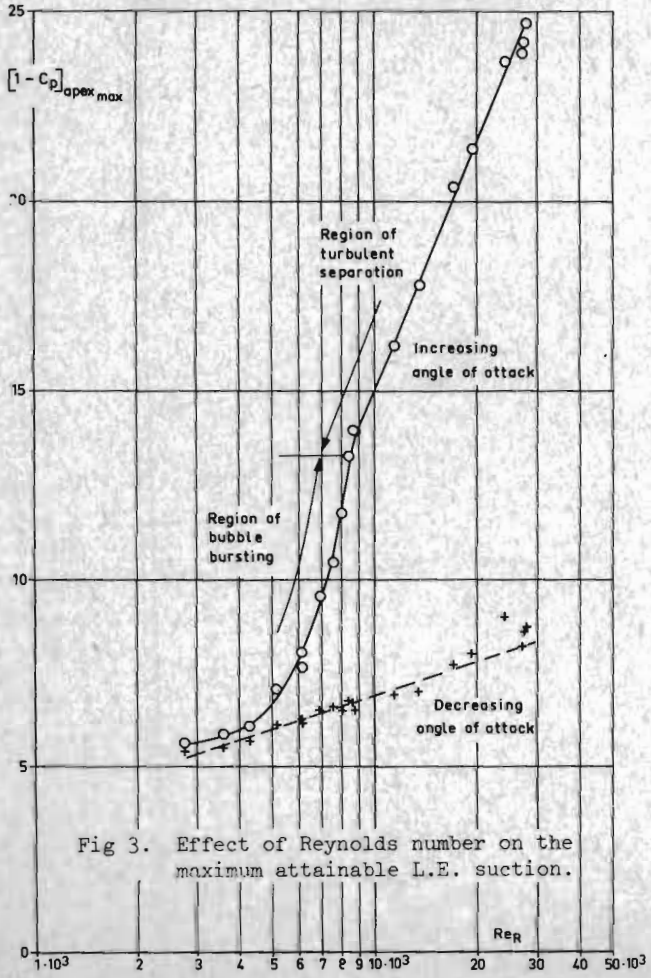

Fig 3. Effect of Reynolds number on the maximum attainable L.E. suction.

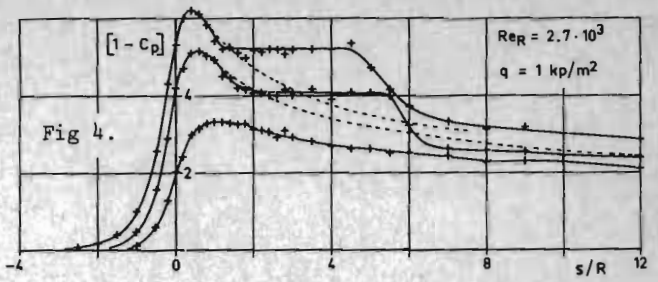

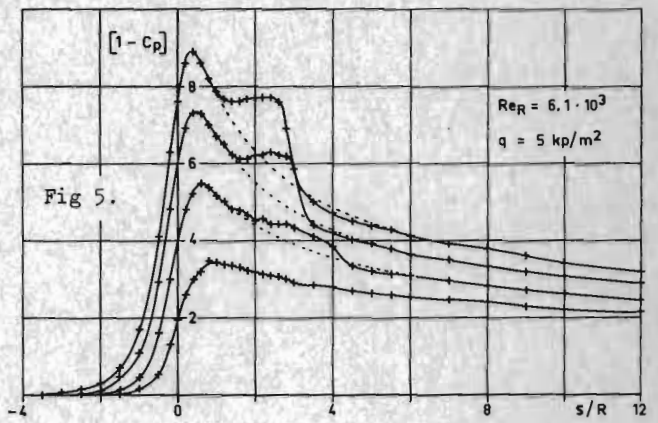

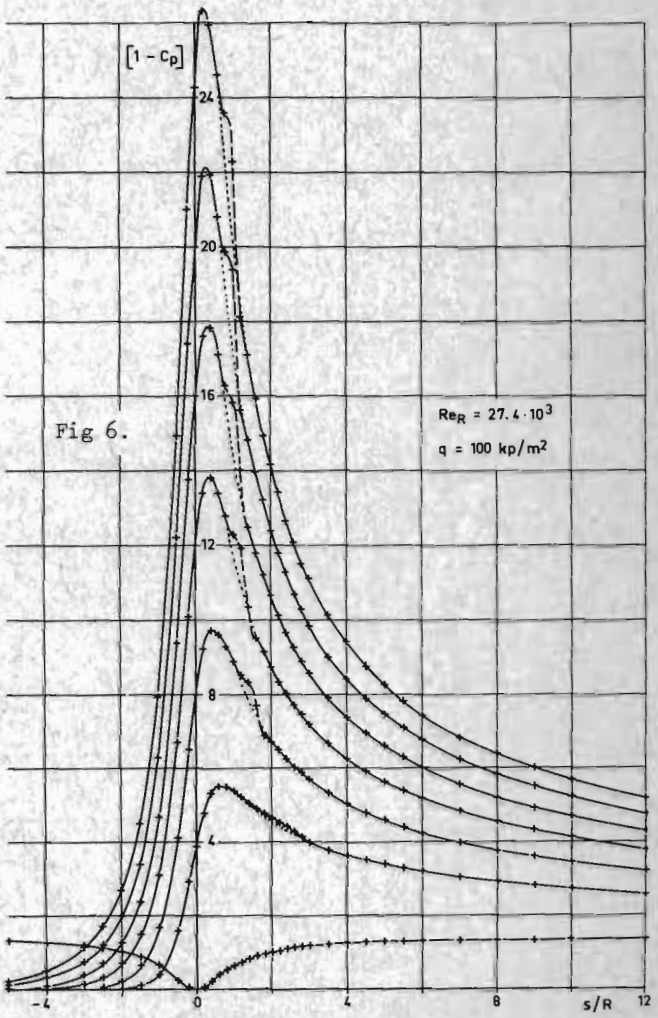

Figs 4-6. Effects of the magnitude of the circulatory flow around a L.E. on the pressure distribution.

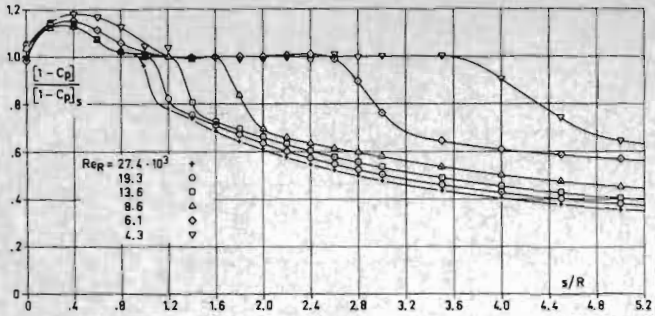

Fig 7. Relative pressure distributions of the laminar separation bubbles at near maximum L.E. suction vs surface contour.

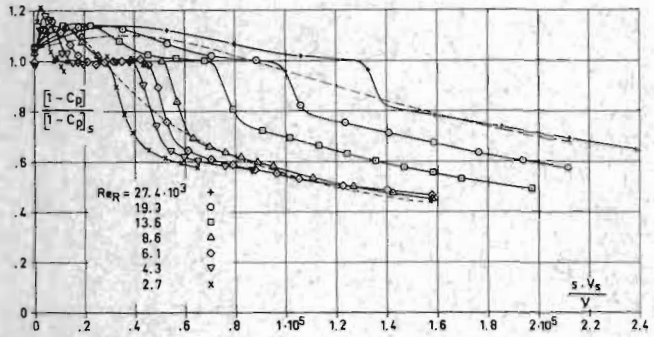

Fig 8. Relative pressure distributions of the laminar separation bubbles at near maximum L.E. suction vs local Re.

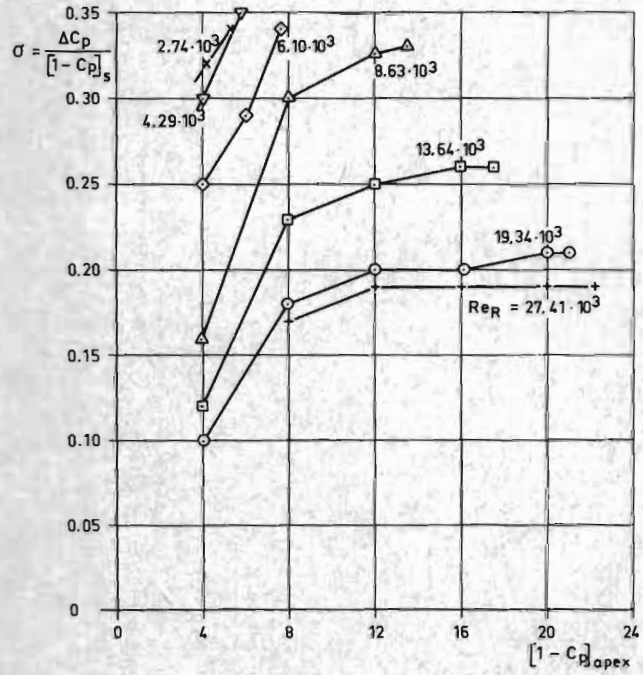

Fig 9. Pressure rise coefficients for laminar separation bubbles vs $[1-C_p]_{apex}$ at different Re.

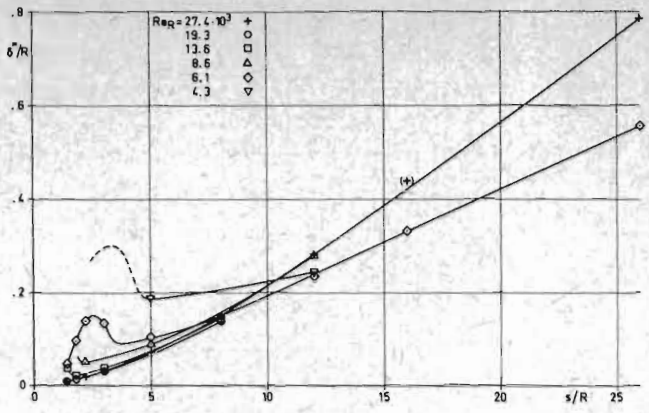

Fig 10. Displacement thickness of the boundary layers at near maximum L.E. suction for different Re.

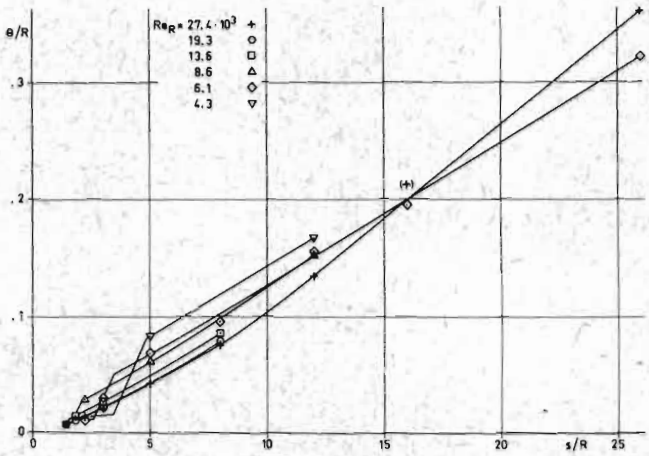

Fig 11. Momentum thickness of the boundary layers at near maximum L.E. suction for different Re.

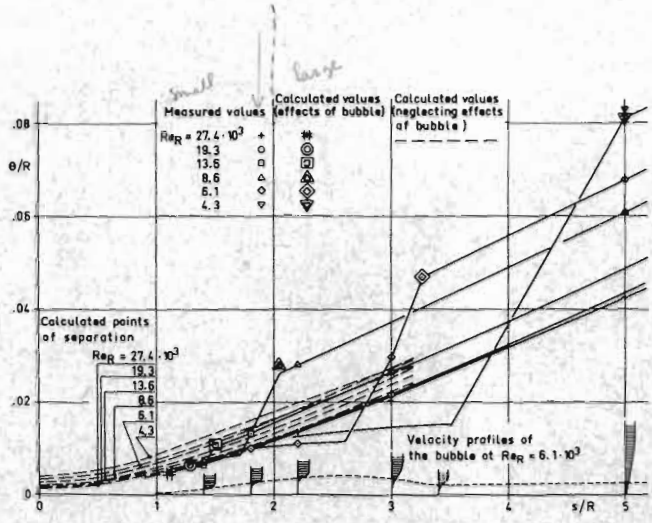

Fig 12. Calculated momentum thickness of the boundary layers for reattaching bubbles.

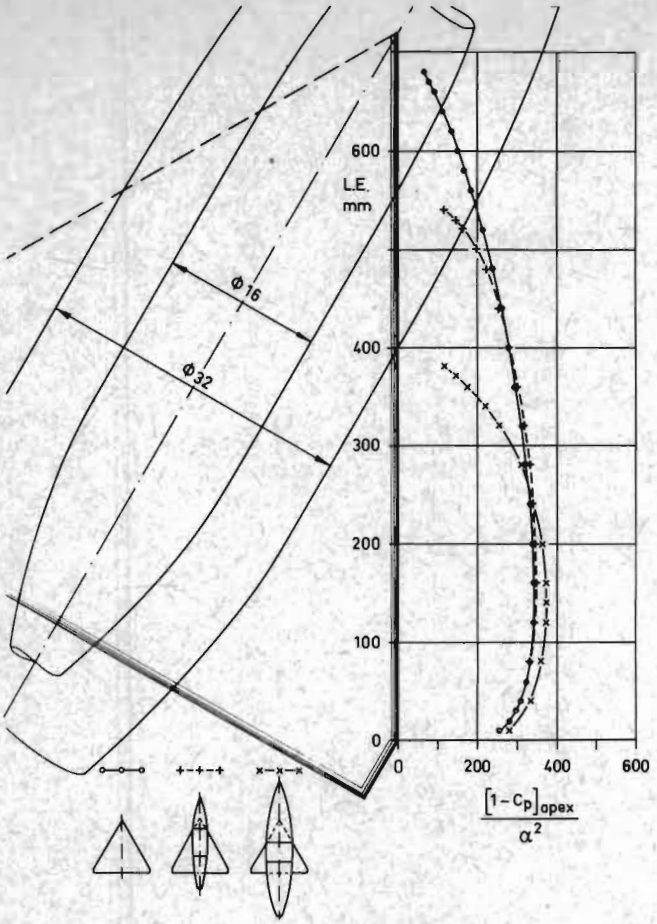

Fig 13. L.E. suction distributions for a 60° Δ-wing including the effect of fuselage.

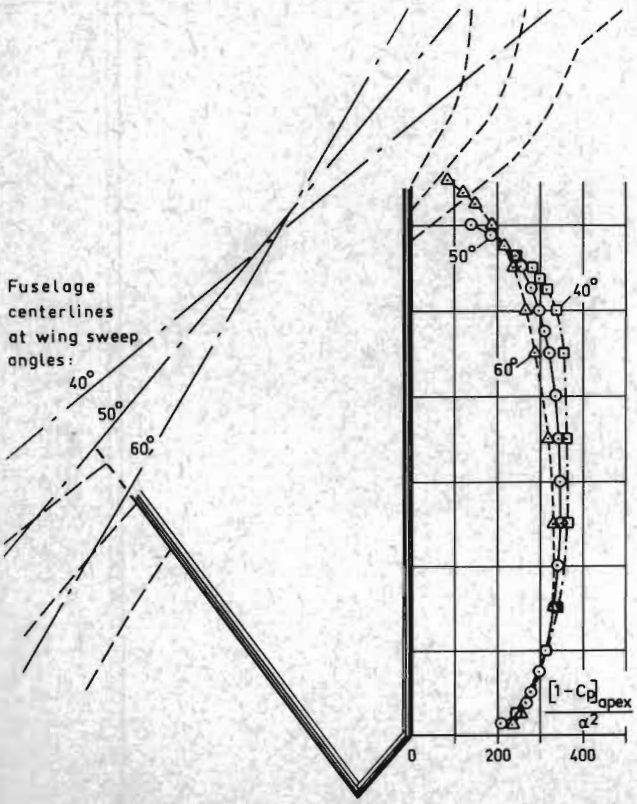

Fig 14. L.E. suction distributions for a swept wing at different sweep angles.

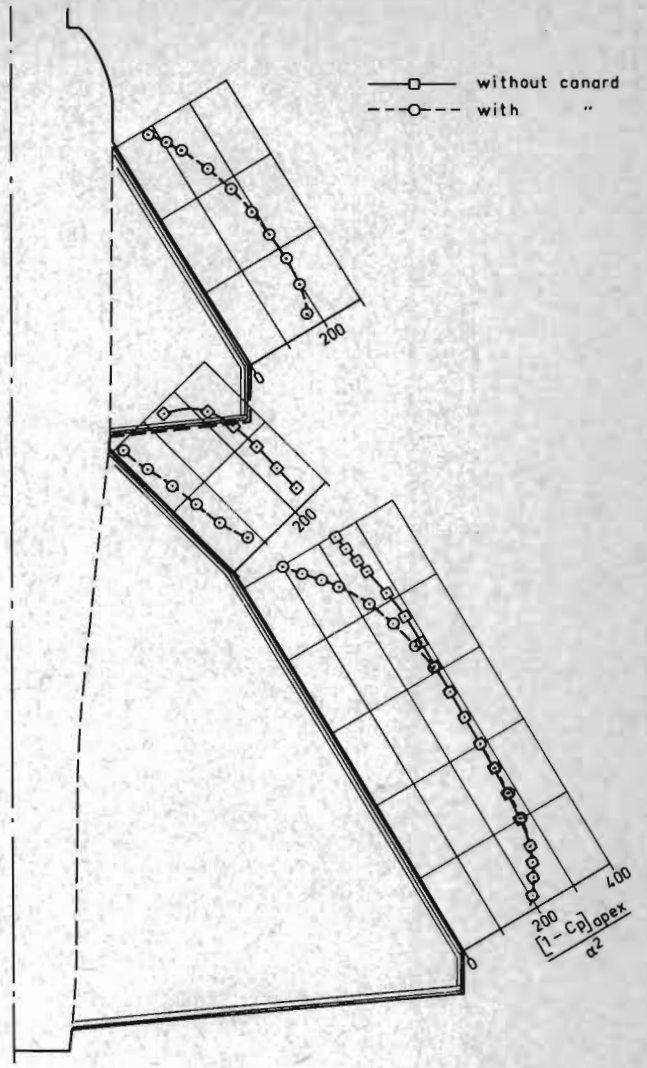

Fig 15. L.E. suction distributions for a Viggen-type configuration including the effect of canard surface.

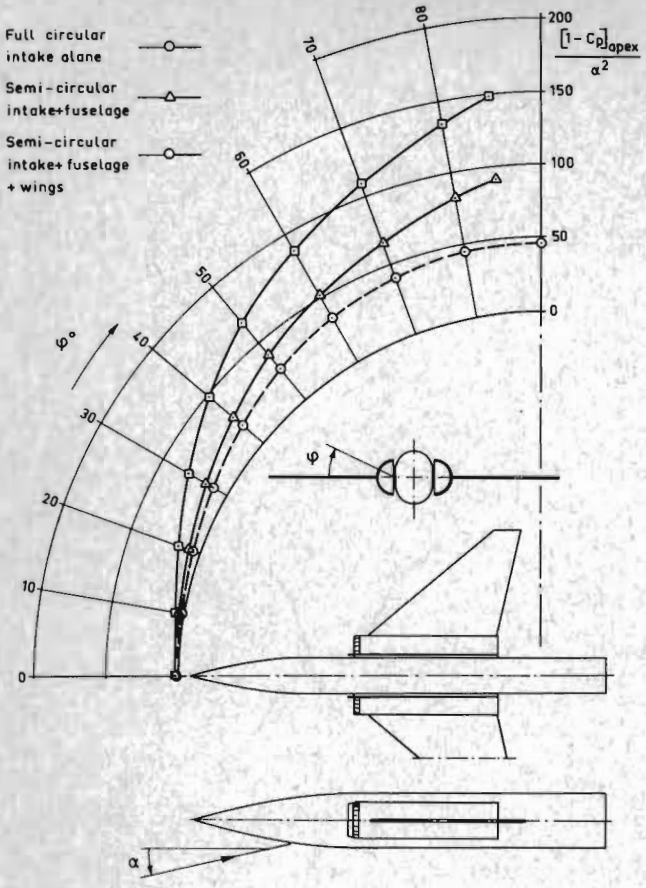

Fig 16. Lip-suction distributions for side-mounted air intakes.

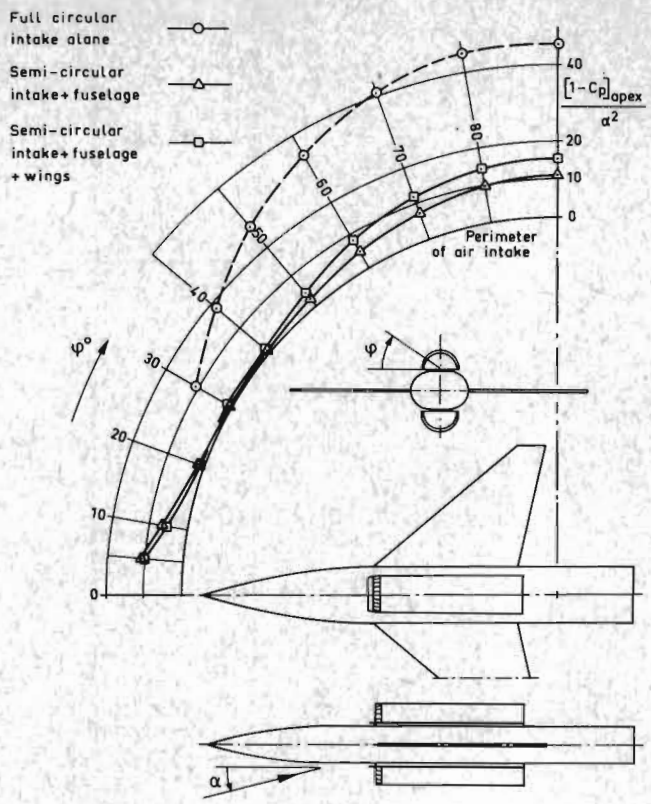

Fig 17. Lip-suction distributions for dorsal or ventral mounted air intakes.

D I S C U S S I O N

V.L. Marshall (British Aircraft Corporation, Weybridge, U.K.); I would suggest that your theoretical presentation of the velocity distribution, and hence pressure coefficients towards leading-edges is in question due to the omission of the presence of compressibility. With the levels of C_p being discussed here, this must affect the rates of expansion and hence real C_p levels?

S.O. Ridder: Compressibility has been considered during the course of the work, but its inclusion does little to influence the definitions of the formation of bubbles, growth etc. in the way that we have been considering them in this paper.